Light: Science & Applications (2013) 2, e60; doi:10.1038/lsa.2013.16

www.nature.com/lsa

ORIGINAL ARTICLE

Mode splitting transmission effect of surface wave excitation through a metal hole array

Lin Chen, Yiming Zhu, Xiaofei Zang, Bin Cai, Zhou Li, Le Xie and Songlin Zhuang

The resonant frequencies of the excited surface waves on a metal hole array with respect to the incident angle were studied in the terahertz region. The experimental and theoretical results demonstrate that the resonant peak of surface wave excitation splits into two when transmitted through a metal hole array off-normally. The high-order mode with resonant frequency above the cutoff frequency f_c (plasma frequency effect) has a shorter attenuation length than that of the low-order mode whose resonant frequency is below f_c. The reason is that the high-order mode is a coupled mode consisting of surface wave and hole modes, while the low-order mode is just an excited surface wave (which can be considered as the spoof surface plasmons). Our investigation may open a door to distinguish the spoof surface plasmons and the coupled modes of surface waves and hole modes.
Light: Science & Applications (2013) **2,** e60; doi:10.1038/lsa.2013.16; published online 29 March 2013

Keywords: angular dependence; cutoff frequency; metal hole arrays; surface waves; terahertz

INTRODUCTION

In recent years, interest in the utilization of terahertz (THz) radiation has increased because of the various applications of THz technology. This trend has led to an increasing demand for THz components that can be used to manipulate THz beams. One of the most promising candidates for use as a component in THz devices is metal hole array (MHA). It has previously been demonstrated that a thin metal plate perforated with an array of periodically spaced holes exhibits bandpass characteristics when irradiated by electromagnetic waves of variable frequency.[1] However, worldwide interest was not sparked until enhanced transmission in the visible region was first experimentally discovered on metal films featuring hole arrays with subwavelength periodicity.[2] Further research theoretically revealed that the physical origin of this enhancement was due to surface plasmon polaritons.[3] At THz frequencies, however, the dielectric properties of metals are those of perfect electric conductors, therefore, there are no surface plasmon polaritons with which to couple.[4] Instead of surface plasmon polaritons, spoof surface plasmon polaritons can form on a metal surface with a designed periodic structure and contribute to an enhancement in transmission.[5] However, the theory of spoof surface plasmon polaritons is limited to arrays with periodicities that are much smaller than the resonant wavelength.

Recently, researchers have found that the main mechanism for enhanced transmission is the excitation of surface waves, which are interfered and scattered by periodically arranged structures.[6,7] Because MHAs are novel candidates for use as components in THz devices, such as filters,[8] optical switches,[9] sensors,[10] *etc.*, the features of MHA surface waves at normal incidence have been investigated in detail by changing parameters such as the number of holes,[11] the hole diameter,[12] the coating thickness of the dielectric film on the metal surface,[13] *etc.* In general, this enhanced transmission characteristic is one type of plasmonic property that has been widely studied in THz plasmonic metamaterial systems,[14–20] which is typically composed of periodically arranged unit cells. More importantly, the mode splitting effect observed in asymmetrical metamaterial systems results from the near-field coupling induced by the strong coupling between a bright eigenmode and a dark eigenmode.[21–24] For example, a bright eigenmode is supported when two-gap split ring resonators are perfectly symmetric and interfere constructively at an identical frequency. When one of the gaps is off-centered, the resonance frequencies of the resonators differ slightly and mode splitting occurs due to destructive interference.[23]

In this study, to better understand the characteristics of surface waves and mode splitting, the relationship between the incident angle and the transmission of surface waves through a MHA structure was investigated. In contrast with the mode splitting of near-field coupling coming from electromagnetically induced transparency in asymmetrical metamaterial systems, the mode splitting effect observed in this study depends on the in-plane component of the incidence vector. In addition, two splitting modes also have different properties: the high-order mode excited by a coupled mode of surface waves and the hole modes has a shorter attenuation length than that of the low-order mode, which is excited just by the spoof surface plasmons. A theoretical model is established to explain these characters. Our results harness the full potential of MHAs, which can find many applications in THz devices.

Engineering Research Center of Optical Instrument and System, Ministry of Education, Shanghai Key Lab of Modern Optical System, University of Shanghai for Science and Technology, Shanghai 200093, China
Correspondence: Professor YM Zhu, Engineering Research Center of Optical Instrument and System, Ministry of Education, Shanghai Key Lab of Modern Optical System, University of Shanghai for Science and Technology, No. 516 Jungong Road, Shanghai 200093, China
E-mail: ymzhu@usst.edu.cn
Received 7 June 2012; revised 27 October 2012; accepted 3 November 2012

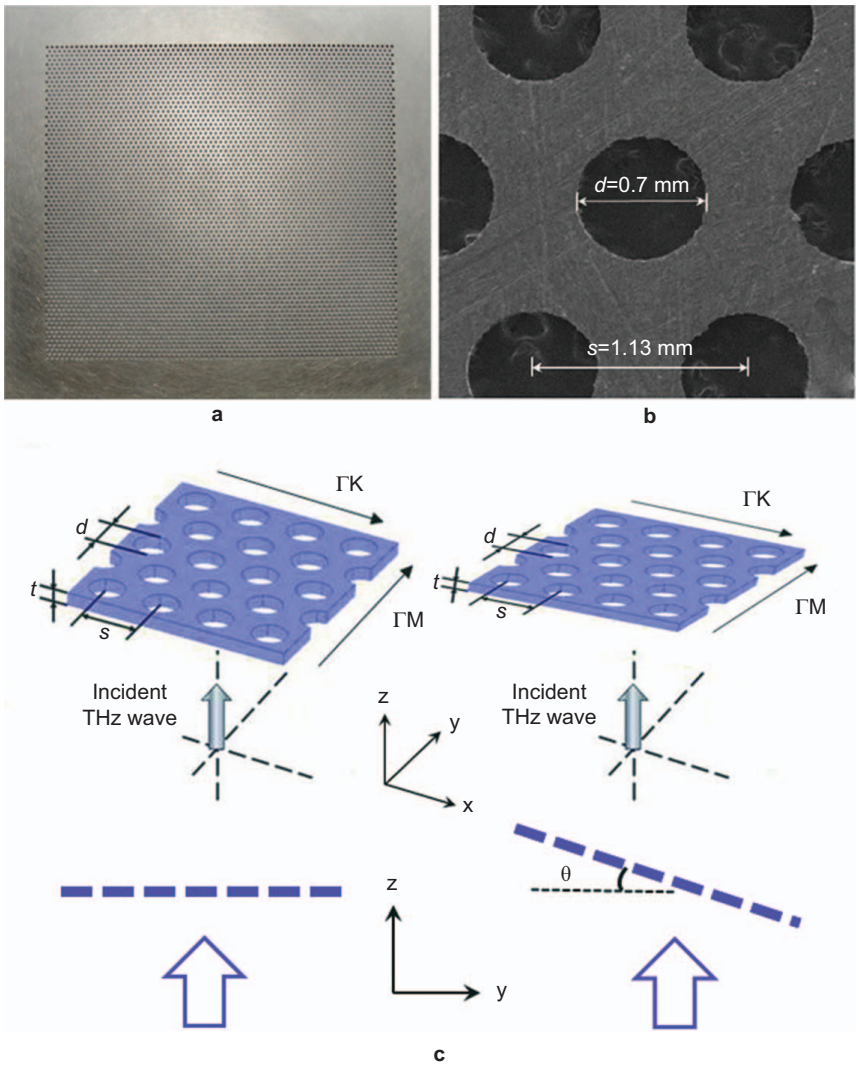

Figure 1 Schematic diagram of a MHA. (**a**) A top view of the MHA slab fabricated on an aluminum plate. (**b**) Scanning electron microscopy image of the MHAs. (**c**) Lattice characteristics. MHA, metal hole array.

MATERIALS AND METHODS

To excite surface waves, we fabricated an aluminum MHA slab as shown in Figure 1a and 1b. Traditional micromachining was used to fabricate the arrays. Using a stepping motor control system, the spacing of the holes can be measured precisely. The MHA slab consisted of a triangular array of circular air holes on a t=250 μm thick, 50 mm× 50 mm rectangular aluminum plate. The holes had a diameter of d=0.7 mm and were arranged on a hexagonal lattice with a pitch of s=1.13 mm. The number of holes was large enough in our structure to avoid the finite size effect.

A transmitted pulse was measured using a THz time domain spectroscopy which was systematically similar to that used in Refs. 25 and 26. A collimated p-polarized THz wave, which was radiated from a 100 fs 800 nm laser pulse pumped photoconductive antenna emitter, was irradiated on the MHA. We rotated the MHA around its ΓK axis, as shown in Figure 1c, to vary the in-plane vector of the incident wave in the ΓM direction. By varying the time delay between the pumping and probe pulses, the waveform of the transmitted THz wave can be measured. An empty air signal was used as a reference for our measurements.

RESULTS AND DISCUSSION

First, for comparison, we studied the MHA at normal incidence (θ=0°). Figure 2a shows the measured transmitted pulse of the reference (air) and MHA at the normal angle. The reference signal (air) was a single-cycle pulse. After inserting the MHA, the signal showed an additional off-plane oscillating attenuation tail, which probably originated from the interaction between the incident waves and the surface waves on the metal surface. To characterize this oscillation, we performed a Fourier transformation to obtain spectra of the frequency domain, as shown in Figure 2b. The resonant peak of the normal incidence is located at 0.265 THz, which agrees well with the results reported in Ref. 10. It is worth noting that the cutoff frequency is 0.251 THz in our structure based on Equation (5) in Ref. 27. According to Pendry's theory, the cutoff frequency represents the marginal value of the spoof surface plasma frequency.[28] The experimental results show that the resonant frequency is larger than the cutoff frequency. Therefore, spoof surface plasmon polariton theory cannot be applied directly to our MHA at normal incidence.

doi:10.1038/lsa.2013.16

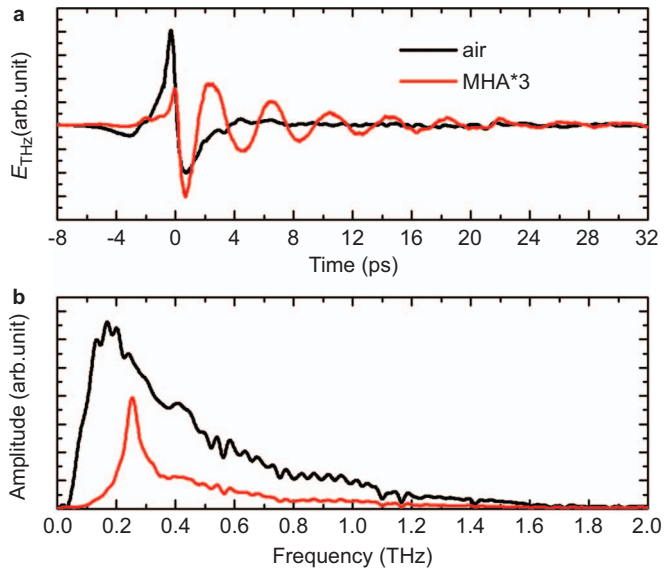

Figure 2 (**a**) The incident and transmitted THz waveform of the MHA at normal incidence. (**b**) Corresponding Fourier-transformed spectra in the frequency domain. MHA, metal hole array; THz, terahertz.

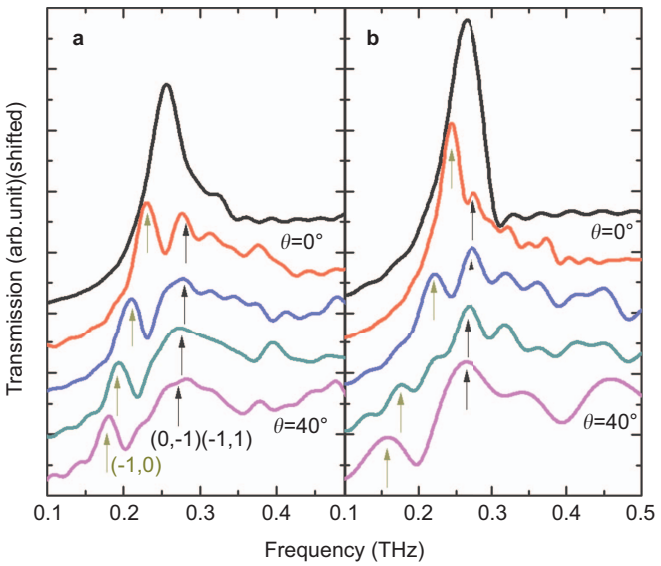

Figure 3 Transmission spectra of the MHA at incident angles ranging from 0° to 40° with a step of 10°. For clarity, each curve was arbitrarily shifted vertically by 0.15. (**a**) Experimental; (**b**) numerical results. MHA, metal hole array; THz, terahertz.

We then conducted an experimental study on the angular-dependent transmission features of the MHA, the results of which are shown in Figure 3a. We found that by changing the incident angle θ, the resonant peak of the surface waves splits into two peaks, one with a lower frequency and the other with a higher frequency relative to the frequency of the non-split peak at an incident angle of 0°. Moreover, the low-frequency peak moved toward lower frequencies as the incident angle increased. We also performed numerical calculations on the transmission spectra using CST software, inputting the same parameters used in the experiment; the results are shown in Figure 3b. The calculation results show similar behavior to those observed in the experiments. We also measured the transmission spectra by rotating the MHA around the ΓM axis to obtain a variation of the in-plane component in the ΓK direction and obtained similar results.

We attribute this phenomenon to the excitation of surface waves. The surface wave vector will couple with the in-plane vector of the incident wave on the MHA slab at a finite incident angle. To quantitatively describe the transmission spectra that dependence on the incident wave vector direction, a surface wave dispersion relationship is used. This dispersion relationship is appropriate for smooth metal/dielectric surfaces, therefore, the influence of the hole arrays was neglected for convenience in performing the calculations. If an incident wave is irradiated on a grating at an angle of θ, the energy and momentum conservation of the coupling effect between the surface wave and the incident wave vector is given by[29]

$$\boldsymbol{k}_{sw}=\boldsymbol{k}_{in}+m\boldsymbol{G}_x+n\boldsymbol{G}_y \quad (1)$$

where $\boldsymbol{k}_{sw}$ is the surface wave vector; $\boldsymbol{k}_{in}=(2\pi f\sin\theta/c)\times(1,0,0)$ is the in-plane vector of the incident wave; m and n are integers; $\boldsymbol{G}_x$ and $\boldsymbol{G}_y$ represent the grating momentum, where, for a hexagonal lattice, $\boldsymbol{G}_x=(2\pi/s)\times(2/(3)^{1/2},0,0)$ and $\boldsymbol{G}_y=(2\pi/s)\times(1/(3)^{1/2},1,0)$; c is the velocity of light in vacuum. The surface wave vector amplitude is equal to $|\boldsymbol{k}_{sw}|=n_{sw}\times 2\pi f/c$, where the effective index $n_{sw}\approx 1$ due to the large permittivity of metals.[30] Thus, we can obtain an equation that describes the conditions under which surface waves are excited:

$$f_{sw}=\frac{2(m^2+mn+n^2)}{\sqrt{(2m+n)^2+3n^2\cos^2\theta}-(2m+n)\sin\theta}\times f_0 \quad (2)$$

where f_{sw} is the resonant frequency of surface waves and f_0 is the lowest surface wave resonance frequency at normal incidence, which is equal to $2c/[(3)^{1/2}s]$.[31] This expression generalizes the relationship between f_{sw} and the incident angle θ, where the resonant formula discussed in Refs. 11–13 is a special case (θ=0°) of this equation. From Equation (2), we can see that the resonant frequency f_{sw} is a function of the incident angle θ. At normal incidence, the resonant frequencies can be calculated as follows:

$$f_{sw}=f_0\sqrt{m^2+mn+n^2} \quad (3)$$

where s=1.13 mm and f_{sw} is 0.307 THz at the lowest mode, slightly higher than the peak frequency observed in Figure 2b. This is similar to the results described in Ref. 11.

When the incident angle θ becomes finite, the lowest mode splits into two branches. These newly emerged branches are excited as a result of the non-zero parallel vector of the incident wave. For an accurate estimate of the shift in surface wave resonances, we analyzed the position of the strongest transmission peak modes, (−1,0) and (0,−1)/(−1,1). Here, the (0,−1) and (−1,1) modes are degenerate, and both have the same dispersion relationship according to Equation (2). The dispersion curves for the surface wave modes (−1,0) and (0,−1)/(−1,1) are displayed in Figure 4. The numerical and experimental results extracted from Figure 3 are also presented.

The experimental results agree well with the numerical results and the results of the calculations performed using Equation (2). From Equation (1), we can also see that $\boldsymbol{k}_{in}$ increases or decreases with the reciprocal vectors, which depend on the incident angle. The in-plane wave vector $\boldsymbol{k}_{in}$ increases with the incident angle θ, leading to a shift in the photonic bands to lower frequencies. The physical origins of this phenomenon lie in the folding of the in-plane Brillouin zone and have been discussed in detail by Ghaemi *et al.*[3] with respect to the visible

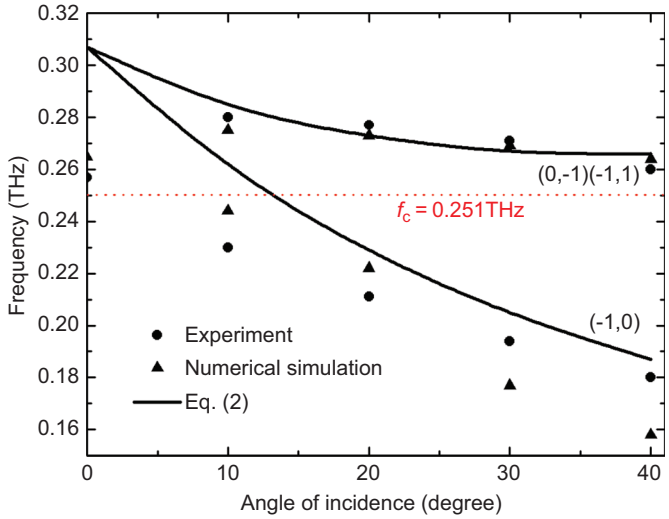

Figure 4 Dispersion relationship of modes (−1,0) and (0,−1)(−1,1). The numerical results were obtained from Figure 3a. The theoretical results (solid line) were calculated using Equation (2). f_c is the cutoff frequency of the MHAs. MHA, metal hole array; THz, terahertz.

range. The splitting characteristics clearly confirm the involvement of surface wave excitation during the transmission process. For high-order peaks beyond 0.4 THz, this splitting characteristic is very weak, as shown in Figure 3. This is because the reciprocal vectors of high-order modes are sufficiently large and less sensitive to the variation of the in-plane vector of the incident wave. All of the results in Figure 4 indicate that the excitation of surface wave plays an extremely important role in influencing the resonant frequency of MHAs.

In Figure 4, we can also obtain that the resonant frequencies of the two splitting modes localized at different sides of the cutoff frequency f_c. To further confirm the generation of the surface wave modes mentioned above, we simulated the electric field distribution map, E_x, on the input and output metal surfaces of the MHA. Periodical boundary conditions and the perfect electrical conductor approximation were used. Figure 5a shows the distribution of E_x at the resonant peak of 0.265 THz of the surface waves at normal incidence. The field pattern presents the opposite symmetry. The intensity of the electric field along the *x*-direction is strongly localized near the circular hole edge and decays gradually along the *z*-direction away from the metal surface. This is because the zero-order diffraction mode becomes apparent at the resonant frequency with the excitation of surface waves. An attenuation length on the order of the incident wavelength can be achieved even though a perfect electric conductor is used.[32] Figure 5b and 5c show the electric field distribution E_x of two resonant frequencies, 0.222 THz ((−1,0) mode) and 0.273 THz ((0,−1)/(−1,1) mode), respectively, at an incident angle of 20°. The simulation results also show a clear intensity modulation of E_x along the *x*-direction within individual holes at both resonant frequencies. However, compared with the E_x at normal incidence, the distributions of E_x on the two surfaces of the hole array interface are asymmetric for the f=0.222 THz map, and this asymmetry is slightly stronger for the f=0.273 THz map. In addition, the spatial attenuation length of the surface wave at a resonant frequency of f=0.222 THz is longer than that of f=0.273 THz. This localized effect is clearly illustrated in the (0,−1)/(−1,1) mode map. The differences between Figure 5b and 5c can be explained by the fact that the MHA has its own cutoff frequency f_c for incident wave propagation. When the (−1,0) order wave with resonant frequency $f_{sw}<f_c$ transmits through the MHA, the air holes can be regarded as barriers. Consequently, the incident wave is converted to an evanescent wave and tunnels through the air holes resonantly. On the contrary, for the (0,−1)/(−1,1) mode whose resonant frequency, f_{sw}, is $>f_c$, the strong coupling between the surface waves and the hole modes should be the dominant mechanism for the transmitted wave.[4] Eventually, we could distinguish spoof surface plasmons from coupled modes by modes splitting effect.

CONCLUSIONS

In summary, we succeeded in investigating the resonant properties of surface waves by using a thick metal material. The resonant mode splitting of the surface waves due to the non-zero in-plane vector of the incident wave was observed and theoretically analyzed. The features of two splitting resonances were observed and distinguished by investigating the electric field distribution of these two modes around the hole edge at the peak transmission frequencies. The E_x distribution that was obtained by CST simulation for the peak transmission clearly confirms that the low-order mode, with $f_{sw}<f_c$, shows an attenuation length that is longer than that of the high-order mode, with $f_{sw}>f_c$. The mechanism of this effect is due to the coupling between the surface waves and the hole modes. These results demonstrate that the spoof surface plasmons and the coupled mode consisting of excited surface mode and the hole mode can be easily distinguished, although both of them are bounded in the surface of the MHA. Furthermore, our research reveals the fact that the physical mechanism of modes splitting in MHAs is different from that of metamaterial systems, even though both of these effects are due to the break of symmetry in broad sense.

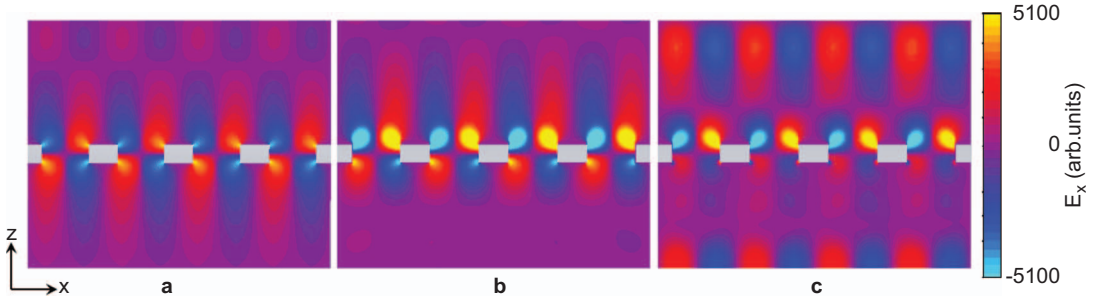

Figure 5 Simulated electric field amplitude E_x of transmission maxima located at (**a**) a resonant frequency of 0.265 THz at normal incidence, (**b**) the (−1,0) mode at a resonant frequency of 0.222 THz at 20° incidence and (**c**) the (0,−1)/(−1,1) mode at a resonant frequency of 0.273 THz at 20° incidence. In all three maps, the electric field antinodes of the surface waves are located around the hole corners for the input and output sides of the hole array. This surface wave distribution allows for the transmission of incident light through the hole array. THz, terahertz.

doi:10.1038/lsa.2013.16

ACKNOWLEDGMENTS

This work is supported by the National Natural Science Foundation of China (11174207, 61138001, 61007059, 61205094), the Key Scientific and Technological Project of Science and Technology Commission of Shanghai Municipality (11DZ1110800), the Major National Development Project of Scientific Instrument and Equipment (2011YQ150021), National Program on Key Basic Research Project of China (2012CB934203) and the Leading Academic Discipline Project of Shanghai Municipal Government (S30502).

1 Chen CC. Transmission of microwave through perforated flat plates of finite thickness. *IEEE Trans Microwave Theor Tech* 1973; **21**: 1–6.
2 Ebbesen T, Lezec H, Ghaemi H, Thio T, Wolff P. Extraordinary optical transmission through sub-wavelength hole arrays. *Nature* 1998; **391**: 667–669.
3 Ghaemi HF, Thio T, Grupp DE, Ebbesen TW, Lezec HJ. Surface plasmons enhance optical transmission through subwavelength holes. *Phys Rev B* 1998; **58**: 6779–6782.
4 Hibbins AP, Lockyear JM, Hooper IR. Waveguide arrays as plasmonic metamaterials: transmission below cutoff. *Phys Rev Lett* 2006; **96**: 073904.
5 Videl FJ, Moreno LM, Ebbesen T, Kuipers L. Light passing through subwavelength apertures. *Rev Mod Phys* 2010; **82**: 729–787.
6 Miyamaru F, Takeda M. Coupling between localized resonance and excitation of surface waves in metal hole arrays. *Phys Rev B* 2009; **79**: 153405.
7 Aigouy L, Lalanne P, Hugonin JP, Julié G, Mathet V *et al*. Near-field analysis of surface waves launched at nanoslit apertures. *Phys Rev Lett* 2007; **98**: 153902.
8 Miyamaru F, Kamijyo M, Hanaoka N. Controlling extraordinary transmission characteristics of metal hole arrays with spoof surface plasmons. *Appl Phys Lett* 2012; **100**: 081112.
9 Hendry E, Lockyear M, Rivas J. Ultrafast optical switching of the THz transmission through metallic subwavelength hole arrays. *Phys Rev B* 2007; **75**: 235305.
10 Miyamaru F, Hayashi S, Otani C, Kawase K. Terahertz surface-wave resonant sensor with a metal hole array. *Opt Lett* 2006; **31**: 1118–1120.
11 Miyamaru F, Hangyo M. Finite size effect of transmission property for metal hole arrays in subterahertz region. *Appl Phys Lett* 2004; **84**: 2742–2744.
12 Tanaka M, Miyamaru F, Hangyo M. Effect of a thin dielectric layer on terahertz transmission characteristics for metal hole arrays. *Opt Lett* 2005; **30**: 1210–1212.
13 Miyamaru F, Tanaka M, Hangyo M. Effect of hole diameter on terahertz surface-wave excitation in metal-hole arrays. *Phys Rev B* 2006; **74**: 153416.
14 Han J, Azad AK, Gong M, Lu XC, Zhang WL. Coupling between surface plasmons and nonresonant transmission in subwavelength holes at terahertz frequencies. *Appl Phys Lett* 2007; **91**: 071122.
15 Qu DX, Grischkowsky D, Zhang WL. Terahertz transmission properties of thin, subwavelength metallic hole arrays. *Opt Lett* 2004; **29**: 896–898.
16 Janke C, Gómez RJ, Schotsch C, Beckmann L, Bolivar P *et al*. Optimization of enhanced terahertz transmission through arrays of subwavelength apertures. *Phys Rev B* 2004; **69**: 205314.
17 Azad AK, Zhao Y, Zhang W. Transmission properties of terahertz pulses through an ultrathin subwavelength silicon hole array. *Appl Phys Lett* 2005; **86**: 141102.
18 Zhang WL, Abul K, Han JG, Xu JZ, Chen J *et al*. Direct observation of a transition of a surface plasmon resonance from a photonic crystal effect. *Phys Rev Lett* 2007; **98**: 183901.
19 Zhang W. Resonant terahertz transmission in plasmonic arrays of subwavelength holes. *Eur Phys J* 2008; **43**: 1–18.
20 Tian Z, Singh R, Han J, Gu JP, Xing Q *et al*. Terahertz superconducting plasmonic hole array. *Opt Lett* 2010; **35**: 3586–3588.
21 Singh R, Rockstuhl C, Lederer F, Zhang WL. Coupling between a dark and a bright eigenmode in a terahertz metamaterial. *Phys Rev B* 2009; **79**: 085111.
22 Singh R, Al-Naib IA, Koch M, Zhang WL. Sharp Fano resonances in THz metamaterials. *Opt Express* 2011; **19**: 6312–6319.
23 Cao W, Singh R, Al-Naib IA, He MG, Taylor AJ *et al*. Low-loss ultra-high-Q dark mode plasmonic Fano metamaterials. *Opt Lett* 2012; **37**: 3366–3368.
24 Singh R, Al-Naib IA, Yang YP, Chowdhury DR, Cao W *et al*. Observing metamaterial induced transparency in individual Fano resonators with broken symmetry. *Appl Phys Lett* 2011; **99**: 201107.
25 Zhu YM, Unuma T, Shibata K, Hirakawa K. Power dissipation spectra and terahertz intervalley transfer gain in bulk GaAs under high electric fields. *Appl Phys Lett* 2008; **93**: 232102.
26 Zhu YM, Unuma T, Shibata K, Hirakawa K, Ino Y *et al*. Femtosecond acceleration of electrons under high electric fields in bulk GaAs investigated by time-domain terahertz spectroscopy. *Appl Phys Lett* 2008; **93**: 042116.
27 Winnewisser C, Lewen F, Helm H. Transmission characteristics of dichroic filters measured by THz time-domain spectroscopy. *Appl Phys A* 1998; **66**: 593–598.
28 Pendry JB, Martin-Moreno L, Garcia-Vidal FJ. Mimicking surface plasmons with structured surfaces. *Science* 2004; **305**: 847–848.
29 Raether H. *Surface Plasmons on Smooth and Rough Surfaces and on Gratings*. Berlin: Springer-Verlag, 1988.
30 Ordal MA, Long LL, Bell RJ, Bell SE, Bell RR *et al*. Optical properties of the metals Al, Co, Cu, Au, Fe, Pb, Ni, Pd, Pt, Ag, Ti, and W in the infrared and far infrared. *Appl Opt* 1983; **22**: 1099–1119.
31 Jiang YW, Tzuang LD, Ye YH, Wu YT, Tasi MW *et al*. Effect of Wood's anomalies on the profile of extraordinary transmission spectra through metal periodic arrays of rectangular subwavelength holes with different aspect ratio. *Opt Express* 2009; **17**: 2631–2637.
32 Veronis G, Fan S. Modes of subwavelength plasmonic slot waveguides. *J Lightw Technol* 2007; **25**: 2511–2521.